This article has been accepted for inclusion in a future issue of this journal. Content is final as presented, with the exception of pagination.

1

IEEE JOURNAL OF SELECTED TOPICS IN APPLIED EARTH OBSERVATIONS AND REMOTE SENSING

Assessment of CYGNSS Wind Speed Retrieval Uncertainty

Christopher S. Ruf, *Fellow, IEEE*, Scott Gleason, *Senior Member, IEEE*, Darren S. McKague, *Member, IEEE*

Abstract— **Measurements of near surface wind speed made by the CYGNSS constellation of GNSS-R satellites are evaluated and their uncertainty is assessed in two ways. A bottom-up assessment begins with a model for the error in engineering measurements and propagates that error through the wind speed retrieval algorithm analytically. A top-down assessment performs a statistical comparison between CYGNSS measurements and coincident "ground truth" measurements of wind speed. Results of the two approaches are compared. Overall performance, as determined by the top-down method, is decomposed using the bottom-up approach into its contributing sources of error. Overall RMS uncertainty in the CYGNSS retrievals is 1.4 m/s at wind speeds below 20 m/s. At higher wind speeds, an increase in the retrieval error is primarily caused by a decrease in the sensitivity of the ocean scattering cross section to changes in wind speed. In tropical cyclones, retrieval errors are compounded by unaccounted departures from a fully developed sea state. Overall RMS uncertainty in the CYGNSS retrievals is 17% at wind speeds above 20 m/s.**

Index Terms— **CYGNSS, Geophysical Model Function, GNSS-R, Ocean Surface Wind Speed**

I. INTRODUCTION

Assessments of the uncertainty in remotely sensed estimates of geophysical parameters from space often follow one of two approaches. A bottom-up approach tracks the estimate from initial engineering measurement through sensor calibration and geophysical retrieval algorithm. Each step is modeled and the associated sources of error quantified, resulting in a propagation of errors calculation of the expected performance. This approach has the advantage of identifying and characterizing individual contributors to the overall uncertainty. Such an error budget can, for example, be useful as a guide to direct future work toward improvements in the largest, driving, sources of error. An alternative, top-down, approach compares the retrieved geophysical parameter to an independent measurement of the same parameter which is matched up to be nearly coincident in time and space. The most common method of comparison used is the root mean square (RMS) difference between them, averaged over a large population of matchups. Retrieval uncertainty is extracted by decomposing the RMS difference into its individual contributors: errors in the independent measurement, any spatial or temporal decorrelation because the two measurements were not made at the same time or averaged over the same spatial region, and the retrieval uncertainty in question. The top-down approach is useful as an end to end assessment of retrieval performance and, when combined with the bottom-up assessment, can serve to validate the error model on which it is based.

Previous spaceborne measurements of ocean surface winds have been evaluated using both bottom-up [1] and top-down [2], [3], [4] approaches. In general, the top-down approach is more common, especially with more mature remote sensing techniques for which the bottom-up error budget is reasonably well understood and the focus is usually on validating the performance of a particular new sensor. In the case of GNSS-R measurements of near-surface ocean wind speed, previous spaceborne missions have been primarily technology demonstrations and their top-down assessments have focused on showing that the measurements were possible [5], [6]. The Cyclone Global Navigation Satellite System (CYGNSS) is the first GNSS-R mission driven by scientific objectives, namely the frequent measurement of near-surface ocean wind speed in and near tropical cyclones [7]. In support of those objectives, a more comprehensive assessment of measurement uncertainty is developed here, including both bottom-up and top-down analyses.

The CYGNSS mission consists of eight spacecraft dispersed around a common low Earth orbit at 35 deg inclination and 520 km altitude. Each spacecraft carries a 4-channel GNSS-R radar receiver capable of measuring Global Positioning System (GPS) L1 signals scattered from the ocean surface [8]. Those received signals are first calibrated into Level 1 (L1) measurements of bistatic radar cross section [9], [10], from which the L1 observables of normalized bistatic radar cross section (NBRCS) and Leading Edge Slope (LES) are derived. The L1 observables are then used to retrieve Level 2 (L2) estimates of the 10 m referenced wind speed above the ocean

This article has been accepted for inclusion in a future issue of this journal. Content is final as presented, with the exception of pagination.

2

IEEE JOURNAL OF SELECTED TOPICS IN APPLIED EARTH OBSERVATIONS AND REMOTE SENSING

surface (u_{10}) [11]. A detailed description of the mission and of the algorithms associated with production of its L1 and L2 science data products is provided in [12]. The work presented here examines bottom-up and top-down assessments of the uncertainty in both the L1 NBRCS and LES and the L2 wind speed products. Particular attention is paid to the performance at the low NBRCS and LES values and high wind speeds encountered in tropical cyclones. One primary objective of this work is an assessment of performance relative to mission level requirements on wind speed measurement uncertainty of +/- 2 m/s at wind speeds below 20 m/s and +/-10% at wind speeds above 20 m/s.

II. LEVEL I CALIBRATION OF OCEAN SURFACE SCATTERING CROSS SECTION

CYGNSS Level 1 calibration is performed in two steps. First, Level 0 measurements by the on-board instrument are converted from units of raw digital counts to a Level 1a Delay Doppler map (DDM) of signal power in units of Watts. This is performed using an estimate of the individual DDM noise floor, a near-time coincident black body calibration load noise power estimate and pre-launch instrument noise calibration tables which characterize the instrument noise power variations with temperature. Second, the L1a DDM is converted to a Level 1b DDM of BRCS values by an unwrapping of the other terms appearing in the bistatic radar equation. The primary correction terms in the L1b calibration include the transmitter effective isotropic radiated power (EIRP), the receive antenna gain pattern and the transmit path loss.

After calibration, a 3 delay bin by 5 Doppler bin sub-region of the L1b DDM centered on the specular point is used to derive the two L1 observables. The NBRCS observable is computed as the summation of the L1b DDM over the 3x5 region divided by the effective surface scattering area of the region. The LES observable is computed as the slope of the integrated delay waveform, found by summing across all 5 Doppler bins at each delay value and considering the result as a function of delay only. More details on the Level 1 calibration and error analysis can be found in [9] and [10].

A. Bottom-up estimate of L1a and L1b errors

Bottom up error analysis of the Level 1 calibration was performed using best estimates of the individual terms in the L1a and L1b calibration equations. This consisted, when possible, of performing error analyses on pre-launch measurements of satellite hardware (*e.g.* in the case of the LNA noise power versus temperature characterization) and in

other cases by using component specifications together with models to predict errors (*e.g.* in the case of the impact of spacecraft attitude knowledge uncertainty on receive antenna gain error). Individual term-by-term estimates for all Level 1 error parameters are described in greater detail in [9] and [10].

One significant error term in the L1 calibration is uncertainty in the GPS EIRP, which is caused by errors in knowledge of the GPS transmit power and transmit antenna gain. The EIRP is monitored by a ground based GPS Power Monitor and those measurements are used to reduce the uncertainty in the GPS antenna patterns and in the transmit power of individual GPS satellites [13]. This results in a GPS EIRP uncertainty of 0.24 dB. The combined uncertainty due to all other sources of error in L1 calibration is 0.31 dB. The total L1 uncertainty is the root-sum-square of these two terms, or 0.39 dB [10].

B. Top-down estimate of L1b error

Top-down performance assessments are most often performed of the geophysical parameters estimated by a sensor rather than of its L1 measurements, largely because it can be difficult to obtain accurate, independent estimates of the L1 measurements with which to compare. In the case of CYGNSS, closely spaced satellites often make measurements that should be nearly identical to one another. Differences between the actual measurements can be used to assess many of the errors associated with L1 calibration. This "trailing pair" technique is used here to provide a top-down assessment of the uncertainty in the L1 science data products.

A trailing pair dataset was assembled from measurements made by the CYGNSS constellation during the period 31 July to 23 August 2017. All possible pairs of measurements made by two different spacecraft were considered and only those were selected which meet the following criteria: difference in measurement time < 10 min; difference in specular point location < 5 km; difference in incidence angle of observation < 1 deg. In every case, the two measurements shared the same GPS transmitting satellite. This selection results in a total of ~200,000 pairs of measurements, which represents ~3% of the total number of samples made during this 24 day interval. Suitable trailing pair measurements are found using a variety of possible pairs of the eight satellites in the constellation – typically sequential pairs separated by less than ten minutes around the orbit plane. The tight restrictions on the similarity between the measurements are imposed to ensure that observations are made of a nearly identical ocean surface at the same measurement geometry. Scatterplots of the measurements by one satellite vs. the other for both NBRCS and LES L1 observables are shown in Fig. 1.
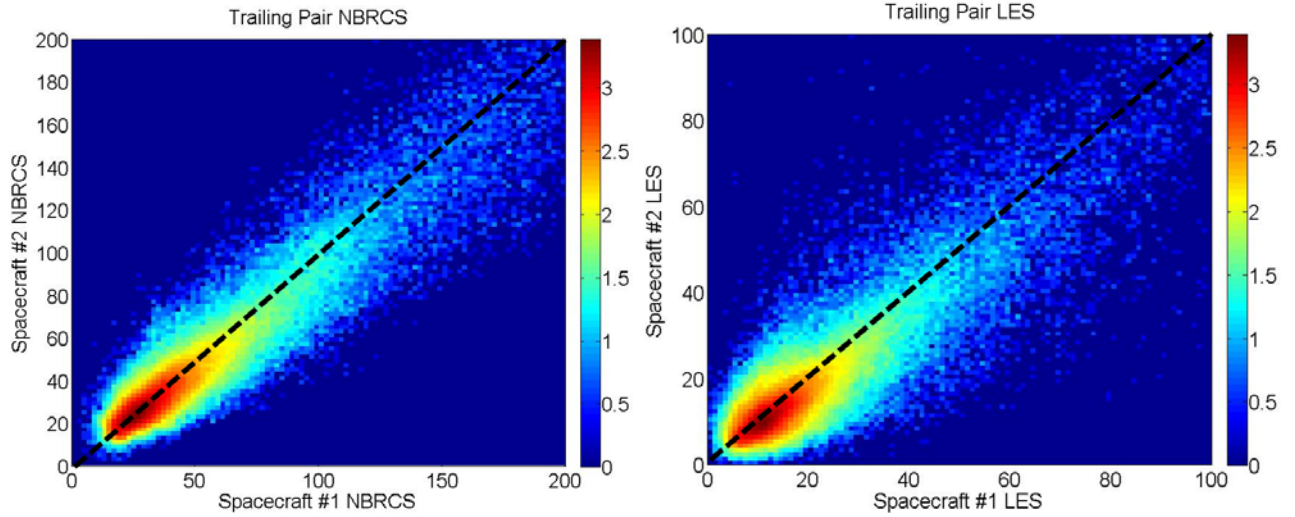
This article has been accepted for inclusion in a future issue of this journal. Content is final as presented, with the exception of pagination.

3

IEEE JOURNAL OF SELECTED TOPICS IN APPLIED EARTH OBSERVATIONS AND REMOTE SENSING

Fig. 1. *Trailing pair log(density) scatterplots of (left) normalized bistatic radar cross section (NBRCS) and (right) leading edge slope (LES) measurements by CYGNSS The diagonal black dashed line is the line of 1:1 agreement. The color scale is the $\log_{10}$ of the number density of points*

The highest density of samples lies along the 1:1 center line in both plots, as expected. The statistical spread of the difference between the pair of measurements quantifies the measurement error due to all sources other than those related to knowledge of the GPS transmission characteristics (i.e. the GPS EIRP), which are common to both measurements. Histograms of the difference are show in Fig. 2. Note that Fig. 1 shows the numeric data values themselves whereas Fig. 2 shows the relative differences in units of dB.

The RMS values of the relative differences, estimated from the populations shown in Fig. 2, are 0.48 dB and 0.71 dB for the NBRCS and LES observables, respectively. Since these are differences between two spacecraft measurements with independent measurement noise and calibration errors, the

Fig. 2. *Trailing pair difference histograms of normalized bistatic radar cross section (top) and leading edge slope (bot) measurements by CYGNSS.*

uncertainty in one of the measurements is lower by a factor of √2. Therefore, the top-down estimate of uncertainty in L1 measurements due to all factors other than error in knowledge of the GPS EIRP is given by 0.34 dB (NBRCS) and 0.50 dB (LES).

C. Comparison of bottom-up and top-down results

The bottom-up error budget discussed in Section II.A above specifies 0.31 dB as the bottom-up estimate of measurement uncertainty in NBRCS due to all noise and calibration error effects other than GPS EIRP. This compares favorably to the top-down estimate of 0.34 dB found using the trailing pair method. The larger error in the case of the top-down estimate may be a result of larger actual errors than were assumed in the bottom-up analysis, or they may result from small differences in the ocean surface scattering cross section given the separations between pairs of observations of up to 10 min and 5 km. A conservative approach is to assume the top-down value of 0.34 dB as an upper bound on the uncertainty. Combining it via root-sum-square addition with the GPS EIRP uncertainty of 0.24 dB noted in Section II.A gives the total uncertainty in NBRCS. Likewise, the trailing pair estimate of LES uncertainty of 0.50 dB should also be combined via root-sum-square addition with the GPS EIRP uncertainty. The resulting total uncertainties in the L1 observables are given by

$$\text{NBRCS RMS uncertainty} = 0.42 \text{ dB} \qquad (1)$$
$$\text{LES RMS uncertainty} = 0.55 \text{ dB}$$

III. LEVEL 2 RETRIEVAL OF WIND SPEED

The CYGNSS mission's baseline wind speed retrieval algorithm, used to produce its Level 2 wind speed science data product, is described in detail in [11]. In summary, the algorithm uses Geophysical Model Functions (GMFs) which relate u_{10} to the L1 observables, NBRCS and LES. The GMFs are derived empirically from a large population of coincident CYGNSS L1 measurements and independent estimates of u_{10} made by either numerical weather prediction models, at low to
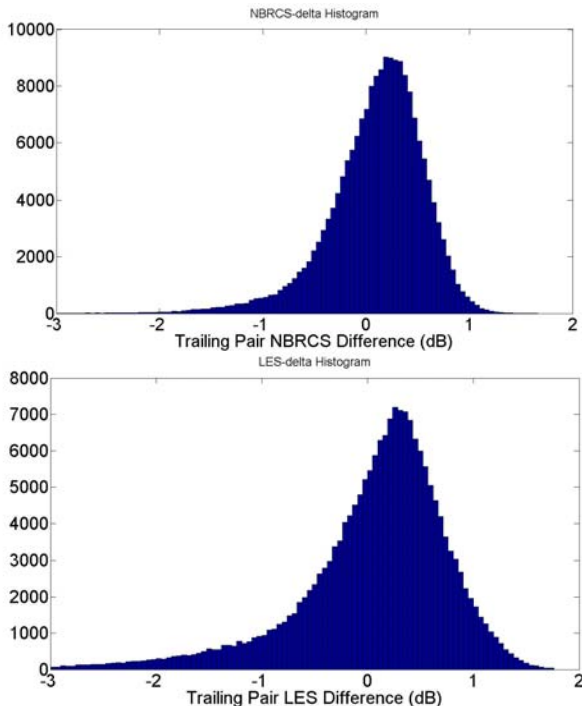
This article has been accepted for inclusion in a future issue of this journal. Content is final as presented, with the exception of pagination.
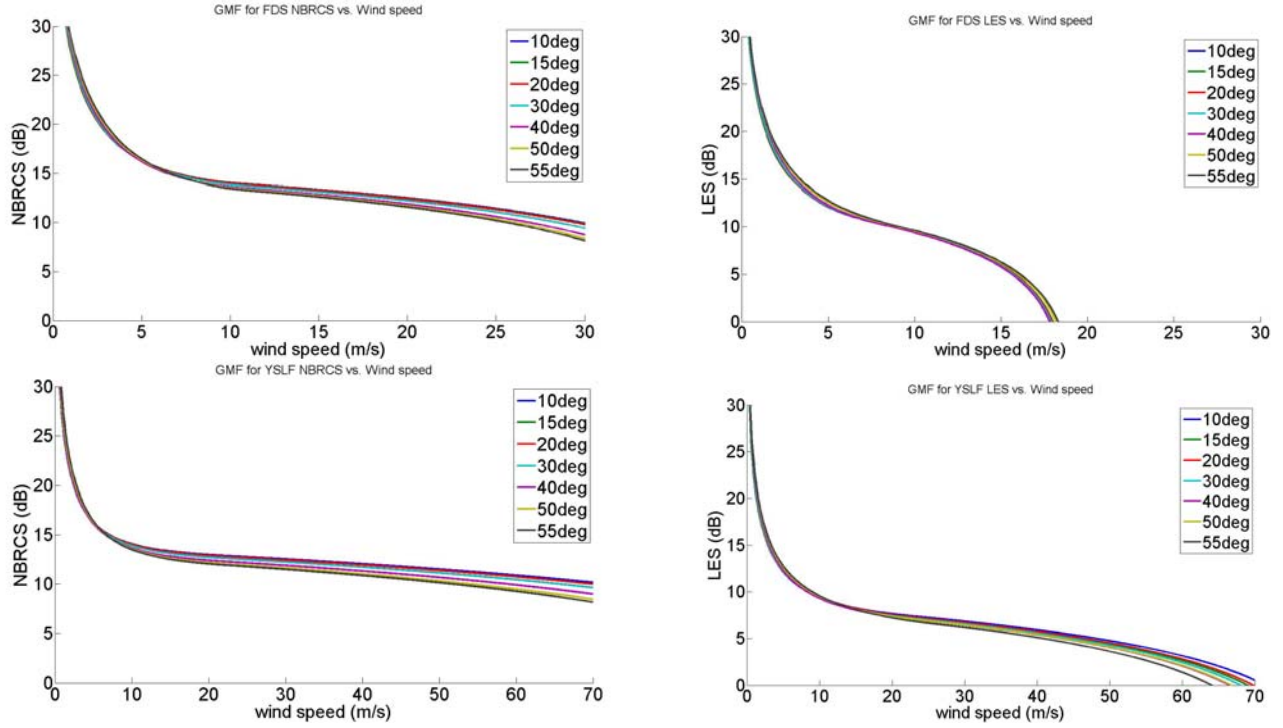
4

Fig. 3. *Geophysical Model Functions at low-to-moderate wind speeds in fully developed seas (FDS) (top row) and high wind speeds in young seas with limited fetch (YSLF) conditions (bottom row) for the L1 observables NBRCS (left column) and LES (right column) at incidence angles of 10, 15, …, 55 deg*

moderate wind speeds, or instruments on NOAA P-3 hurricane hunter aircraft, at high wind speeds [14]. The low-to-moderate wind versions are referred to as the Fully Developed Seas (FDS) GMFs and the high wind versions as the Young Seas/Limited Fetch (YSLF) GMFs. They differ as a result of the sensitivity of the measurements to long wave swell, which tends to be significantly more under-developed in the high wind conditions experienced in tropical cyclones.

Each GMF provides a unique mapping from u_{10} to an L1 observable and the retrieval algorithm inverts it given a measurement of the observable. This produces two estimates of u_{10}, one for each observable, and they are combined together by a minimum variance estimator to produce the final wind speed estimate [15]. Examples of the FDS GMFs, for low to moderate wind speeds, for both L1 observables are show in Fig. 3(top), and the YSLF GMFs at high wind speeds are shown in Fig. 3(bot).

Several features of the GMFs are noteworthy. At wind speeds below 5-10 m/s, the slope of the GMF ($dObs/du_{10}$) becomes very steep and small changes in wind speed correspond to large changes in the L1 observable. The component of wind speed retrieval error that is dependent on measurement error can be expected to be lowest in this regime. At higher wind speeds, the slope decreases markedly. The value of u_{10} at which this transition occurs differs for the two observables and also depends weakly on incidence angle. The component of wind speed error due to measurement error will be higher here.

A. Bottom-up estimate of L2 uncertainty

Bottom-up construction of an error model for the retrieved L2 wind speed consists of two parts. The uncertainty in measurement of the L1 observables, due both to measurement

noise and calibration error, is scaled to a corresponding error in the wind speed using a propagation-of-errors analysis. Intrinsic error in the wind speed retrieval algorithm is also considered. Intrinsic error represents retrieval error that would have been present even if the measurements had been perfect. It accounts for such things as the dependence of the observable on other geophysical variables than wind speed which are not properly accounted for in the retrieval algorithm, or a non-unique mapping from wind speed to the observable. These two error sources are considered to be statistically independent and their RMS errors are combined by root-sum–square addition to produce the overall bottom-up uncertainty.

For small errors in the L1 observable, the corresponding wind speed retrieval error can be estimated by linearizing the GMF. The resulting wind speed retrieval error is given by

$$\varepsilon_{Obs}(u_{10}) = \left|\frac{dObs}{du_{10}}\right|^{-1} \varepsilon(Obs) \qquad (2)$$

where ε(Obs) is the RMS error in either the NBRCS or LES observable, and the functional dependence of the observable on u_{10} as shown in Fig. 3. The values of the error are stated in eqn. (1). The slopes of the GMFs ($dObs/du_{10}$) for both L1 observables are shown in Fig. 4(top) for the low-to-moderate wind speed case and the slopes at high wind speeds are shown in Fig. 4(bot). Results are only shown for an incidence angle of 30 deg but the sensitivity is very similar at other angles.

In both FDS and YSLF conditions, the NBRCS observable typically has a higher sensitivity to wind speed than does the LES observable. The exception is at wind speeds between ~10 and 18 m/s in the FDS case, where LES sensitivity is slightly higher. Above ~18 m/s in FDS conditions, the LES observable
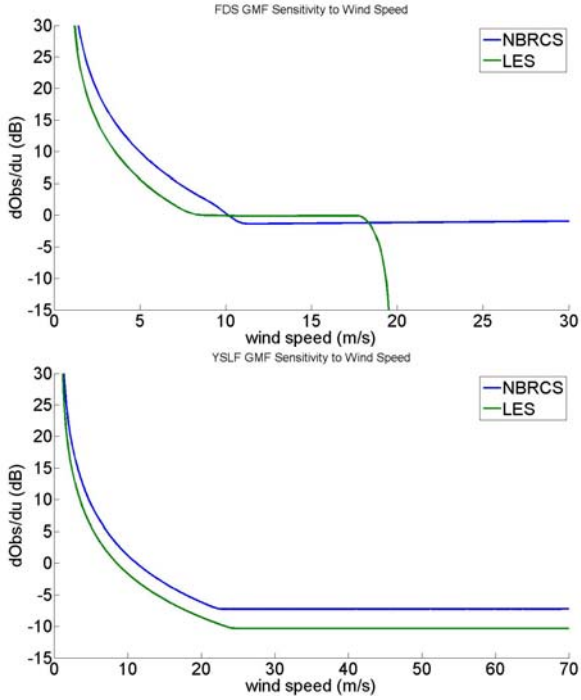
This article has been accepted for inclusion in a future issue of this journal. Content is final as presented, with the exception of pagination.

5

IEEE JOURNAL OF SELECTED TOPICS IN APPLIED EARTH OBSERVATIONS AND REMOTE SENSING

Fig. 4. *Sensitivity (defined as dObs/du$_{10}$) of the (top) FDS GMF and (bot) YSLF GMF to wind speed for L1 observables NBRCS (blue) and LES (green) at an incidence angle of 30 deg.*

becomes very small and effectively loses sensitivity to changes in wind speed. In YSLF conditions, the sensitivity for both observables is low but constant at high (> 25 m/s) wind speeds.

The component of uncertainty in L2 retrieved wind speed due to errors in the L1 observables follows directly from eqns. (1) and (2), using the values of dObs/du$_{10}$ shown in Fig 4. Plots of the resulting values of ε(u$_{10}$) with the NBRCS and LES observables are shown in Figs. 5(top) and 5(mid), respectively. Note that ε(u$_{10}$) is in both cases close to zero at very low wind speeds due to the high sensitivity (large dObs/du$_{10}$) there. Note also that ε(u$_{10}$) becomes very large with the LES observable at wind speeds above ~18 m/s. This is consistent with its loss of sensitivity to wind speed, as seen in Figs. 3 and 4.

The CYGNSS baseline L2 minimum variance (MV) retrieved wind speed is an inverse variance weighted average of the L2 winds derived from the two L1 observables. The component of its uncertainty due to errors in the L1 observables is a similarly inverse variance weighted average of the two ε$_{Obs}$(u$_{10}$) values [13]. In addition, a third component of uncertainty is the intrinsic error in the retrieval algorithm itself, caused by the non-uniqueness of the relationship between u$_{10}$ and the L1 observables. Intrinsic error is estimated using simulated observations produced by an end-to-end simulator (E2ES) [14]. Simulated L1 measurements can be generated by the E2ES as a function of wind speed which are free of calibration errors. The RMS error in MV retrieval performance using these simulated data is found to be 1.3 m/s for wind speeds below 25 m/s. The overall uncertainty in the MV wind speed can be expressed as
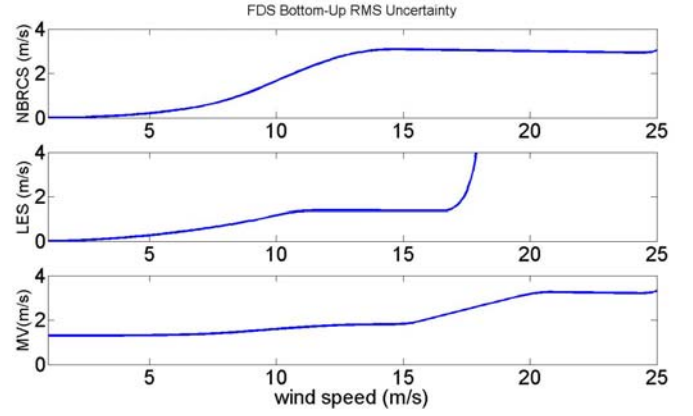

Fig. 5. *Bottom-up L2 wind speed retrieval uncertainty for low-to-moderate wind speeds in fully developed seas. (top) Component due to errors in L1 NBRCS observable; (mid) Component due to errors in L1 LES observable; (bot) Overall uncertainty in minimum variance estimate, including contributions from errors in both L1 observables and from intrinsic error in the retrieval algorithm.*

$$\varepsilon_{MV}(u_{10}) = \left((\varepsilon_{intrinsic})^2 + \left(\frac{1}{(\varepsilon_{NBRCS})^2} + \frac{1}{(\varepsilon_{LES})^2} \right)^{-1} \right)^{0.5} \quad (3)$$

where ε$_{intrinsic}$ = 1.3 m/s and ε$_{NBRCS}$ and ε$_{LES}$ are given by eqn. (2) and shown in Figs. 5(top, mid). The resulting bottom-up uncertainty in the minimum variance retrieved wind speed, ε$_{MV}$, is shown in Fig. 5(bot). At low wind speeds, contributions from L1 measurement error are small and the MV retrieval uncertainty is dominated by the intrinsic error. Above ~10 m/s, MV uncertainty begins to increase as the contributions from L1 measurement error become significant. Above ~18 m/s, the LES observable loses sensitivity to wind speed and the MV uncertainty is dominated by errors in the measurement of NBRCS.

A bottom-up estimate of L2 wind speed uncertainty for high wind retrievals using the YSLF GMF follows the same approach, with the appropriate YSLF sensitivity values shown in Fig 4b used instead. In and near tropical cyclones, the mission baseline science data product uses YSLF retrievals based only on the NBRCS L1 observable. This is done because of their significantly higher sensitivity at all wind speeds than retrievals based on the LES observable. The bottom-up YSLF uncertainty is shown in Fig. 6. In the figure, results are shown for different time averaging scenarios. The baseline CYGNSS L2 wind speed retrieval algorithm implements a variable amount of along-track averaging to account for changes in spatial resolution with incidence angle that result from the range of time delays and Doppler shifts, centered on the specular point values, which are used to compute the L1 observables [10]. Individual measurements at the highest incidence angles (> 50 deg) have spatial resolution of ~25 km so no additional averaging is performed. Measurements at the lowest incidence angles (< 15 deg) have spatial resolution of ~15 km and n=5 sequential samples are averaged to produce an effective 25 km resolution. Measurements at the center of the field of view (~ 30 deg)

This article has been accepted for inclusion in a future issue of this journal. Content is final as presented, with the exception of pagination.

6

IEEE JOURNAL OF SELECTED TOPICS IN APPLIED EARTH OBSERVATIONS AND REMOTE SENSING
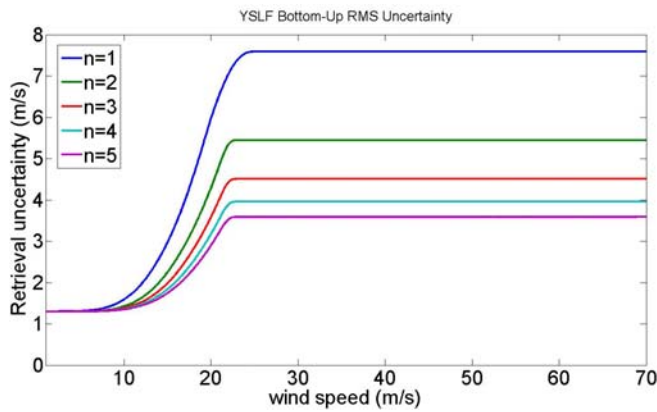

Fig. 6. *Bottom-up L2 wind speed retrieval uncertainty for high wind speeds in young seas with limited fetch. The family of curves represents different numbers, n, of sequential samples averaged together. The number varies to account for the dependence of spatial resolution on incidence angle, with n=1 above 50 deg, n=5 below 15 deg, and n=3 near the center of the field of view at 30 deg.*

have n=3 sequential samples averaged to produce the same effective resolution of 25 km. Averaging reduces the component of L2 retrieval uncertainty due to L1 measurement error but not the intrinsic retrieval error. This is reflected in Fig. 6. At lower wind speeds, the total uncertainty is dominated by the intrinsic component and there is little dependence on the number of samples averaged. At higher wind speeds, L1 measurement errors are dominant and the total uncertainty decreases from 7.6 m/s for a single sample to 4.0 m/s with 4 samples averaged together.

B. Top-down estimate of L2 uncertainty

Top-down assessment of the uncertainty in the L2 data product at low to moderate wind speeds uses near-coincident matchups between CYGNSS measurements and 10m referenced ocean surface wind speeds provided by the European Center for Medium-range Weather Forecasting (ECMWF) Numerical Weather Prediction model [16]. All CYGNSS measurements made during September and October 2017 are used in the analysis. ECMWF winds, reported on a 0.25 deg grid, are bi-linearly interpolated in space and linearly interpolation in time to the location and time of the CYGNSS measurements. Several quality control filters are applied to the matchup data. The ECMWF values are compared to similarly interpolated gridded outputs from the Global Data Assimilation System (GDAS) Numerical Weather Prediction model [17] and a matchup is discarded if ECMWF and GDAS differ by more than 3 m/s. CYGNSS quality control filters include the use of samples that lie in the main beam of the nadir antenna footprint at antenna gain values within ~10 dB of the peak gain. In addition, samples are excluded if the GPS satellite is of block type IIF. These satellites have been found to suffer from considerably more transmit power variability than the earlier block types (IIR and IIR-M). After all quality control filters are applied, the total number of remaining pairs of samples in the matchup population is 30,883,518.

A density scatterplot of the matchup samples is shown in Fig. 7. The scatterplot is logarithmic in number density of samples to more clearly illustrate the distribution of samples
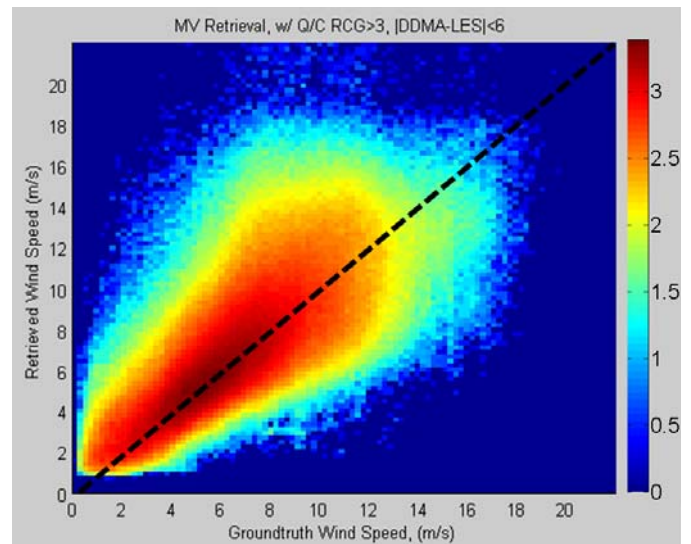

Fig. 7. *Log(density) scatterplot of CYGNSS and matchup ECMWF "ground truth" wind speed samples used for top-down determination of wind speed retrieval uncertainty below 20 m/s. The diagonal black dashed line is the line of 1:1 agreement. The color scale is the $\log_{10}$ of the number density of points.*

both in the region of highest density and in the outlier regions with larger retrieval errors. The highest density of samples occurs along the 1:1 line where ECMWF and CYGNSS winds agree. Asymmetry in the distribution of samples away from the 1:1 line can introduce biases into the retrieval (non zero-mean differences between CYGNSS and ECMWF). Asymmetries can be seen in the figure to increase at higher wind speeds.

The mean and RMS differences between ECMWF and CYGNSS wind speeds are shown in Fig. 8 as a function of (top) ECMWF, (mid) CYGNSS, and (bot) the average of ECMWF and CYGNSS wind speeds. The dependence of the mean difference (or bias) on wind speed is markedly different in each of these three cases. The dependence of bias on ECMWF wind speed is slightly negative at lower wind speeds, has a zero-crossing to positive bias near 9 m/s, and grows increasingly positive at higher wind speeds. Since the bias is reported as (ECMWF – CYGNSS), this indicates that CYGNSS overestimates lower wind speeds and underestimates higher wind speeds. The dependence of bias on CYGNSS wind speed is slightly positive at lower wind speeds, has a zero-crossing to negative bias near 7 m/s, and then grows increasingly negative at higher wind speeds. The difference in sign of the small bias at low wind speeds in Figs. 8(top) and 8(mid) results because, while CYGNSS tends to overestimate low wind conditions (as reported by ECMWF) by several tenths of a meter-per-second, its underestimation at high winds is significantly larger in magnitude, resulting in an overall shift in the low wind bias to several tenths of a meter-per-second positive when sorted by the CYGNSS reported wind. The larger difference in sign and magnitude between Figs. 8(top) and 8(mid) at higher wind speeds results from the larger magnitude of the bias there, which produces a larger swing between sorting options. The dependence of bias on the average of ECMWF and CYGNSS winds shown in Fig. 8(bot)
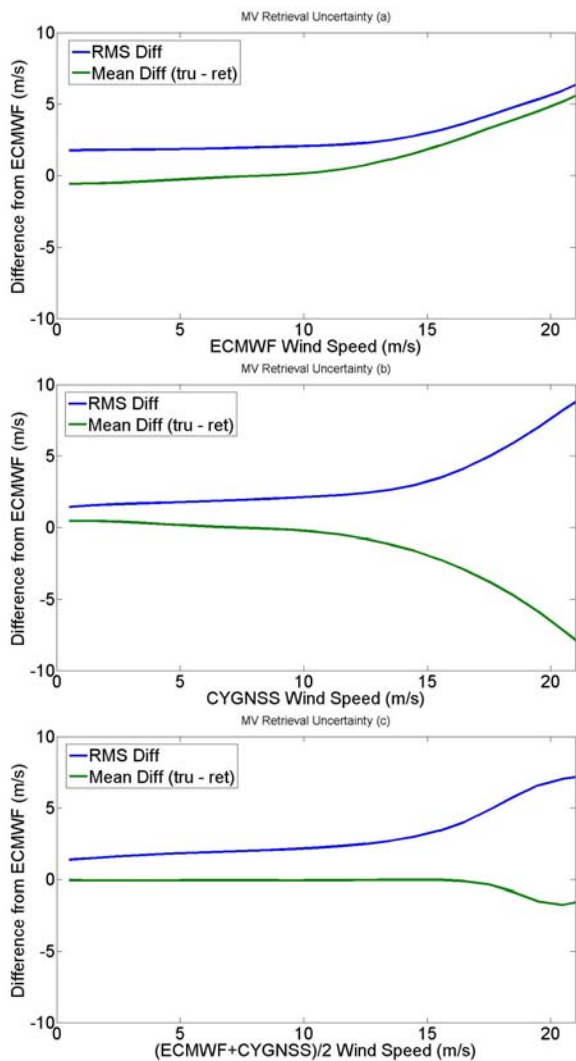
This article has been accepted for inclusion in a future issue of this journal. Content is final as presented, with the exception of pagination.

7

IEEE JOURNAL OF SELECTED TOPICS IN APPLIED EARTH OBSERVATIONS AND REMOTE SENSING

Fig. 8. *RMS and mean difference between matchup CYGNSS and ECMWF wind speeds plotted vs. three difference measurements of wind speed: (top) ECMWF; (mid) CYGNSS; and (bot) the average of ECMWF and CYGNSS.*

lies roughly half way between the other two cases, with negligible bias at low winds and a small negative bias above ~15 m/s.

The behavior of the RMS difference vs. wind speed is similar in all three cases. It includes a primary contribution from the CYGNSS retrieval errors plus smaller secondary contributions from errors in the original ECMWF wind fields and possible errors introduced by the spatial and temporal interpolation process used to align the two data sets. Comparing the bottom-up uncertainty estimate shown in Fig. 5c with the top-down one in Fig. 8 several common traits are evident. The RMS uncertainty rises only gradually with wind speed below ~10 m/s, with values slightly below 2 m/s (the fraction of this value due to CYGNSS will depend on the allocation for errors in ECMWF and in the interpolation). The bottom-up error model attributes this fairly flat dependence to the fact that the intrinsic component of retrieval error is the dominant contributor. The uncertainty rises more steeply above 10 m/s in both cases. The bottom-up error model

attributes the steeper rise to the decreasing sensitivity of the L1 observables to wind speed, and hence the increased sensitivity of the retrieved wind speed to errors in measurement of those observables. RMS uncertainty rises to ~4 m/s at 20 m/s for the bottom-up estimate and ~6 m/s for the top-down estimate. The difference is likely attributable to the bias evident in the top-down comparison, which is small below ~ 12 m/s but increases at higher wind speeds. Bias removal, either algorithmically or through improved calibration of the L1 observables, is a continuing topic of research by the CYGNSS science team. The overall RMS difference, including all samples with ECMWF winds below 20 m/s, is 1.96 m/s. This value is weighted by the distribution of wind speeds in the matchup population, which is approximately Rayleigh distributed with a mean near 7 m/s.

For a top-down estimate of uncertainty at high wind speeds in tropical cyclones, matchups are compiled from twenty-five (25) coincident overpasses of hurricanes by CYGNSS and NOAA P-3 "hurricane hunter" aircraft that occurred during the 2017 Atlantic hurricane season. Coincidence is defined by locating the aircraft ground track during one of its eyewall penetrations that was closest to a CYGNSS specular point track for that overpass and requiring that they occurred within 60 min of one another. The 25 cases identified in this way include overpasses of Hurricanes Harvey, Irma and Maria. Comparison wind speeds were measured by Stepped Frequency Microwave Radiometers (SFMRs) installed on the P-3 aircraft [18]. There are a total of 674 pairs of wind speed samples in this matchup population, which is significantly smaller than the size of the sample population used for low-to-moderate winds.

Estimation of the uncertainty in CYGNSS wind speed retrievals in and near hurricanes is done in two ways, first by qualitatively examining individual hurricane overpasses and examining the impact of time averaging on the retrievals, and second by quantitatively comparing the population of matchup samples. Three examples of hurricane overpasses are shown in Fig. 9. Both the winds retrieved by CYGNSS and measured by the Stepped Frequency Microwave Radiometer (SFMR) on the P-3 are shown. Two versions of the CYGNSS winds are included – one with the standard 1 sec integration time that is performed on-board in real time, and one with a 4 sec running average applied in ground processing. Time-averaging can be seen to considerably reduce the random noise present in the 1 sec values. This is consistent with the behavior predicted by the bottom-up analysis, as illustrated in Fig. 6. With 1 sec averaging (n = 1 in Fig. 6), the RMS uncertainty is estimated to be ~6 m/s. This decreases to ~3 m/s with 4 sec averaging (n = 4 in Fig. 6). One noteworthy characteristic of the overpass matchups shown in Fig. 9, and found in many similar matchups, is the apparent time offset between the SFMR and CYGNSS winds. Minimum and maximum wind speed values and general trends tend to agree more than do second-by-second direct comparisons. This can be explained by the nature of the measurements. The specular point tracks of CYGNSS measurements do not exactly align in position with the P-3 flight tracks, and the time required to sample those
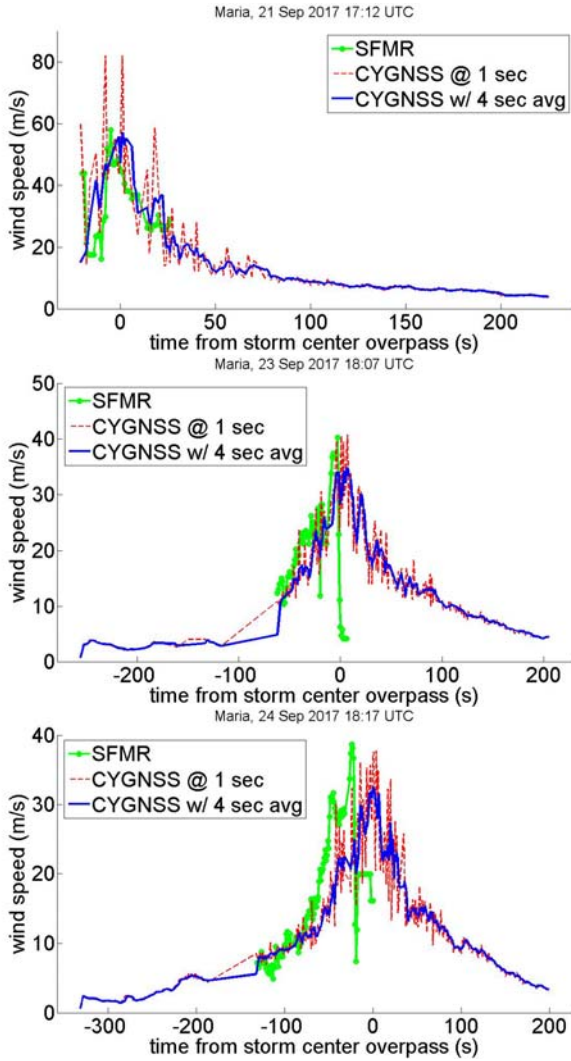
This article has been accepted for inclusion in a future issue of this journal. Content is final as presented, with the exception of pagination.

8

IEEE JOURNAL OF SELECTED TOPICS IN APPLIED EARTH OBSERVATIONS AND REMOTE SENSING

Fig. 9. *Examples of CYGNSS overpasses of Hurricane Maria coincident with NOAA P-3 hurricane hunter aircraft flight on: (top) 21 Sep 2017 at 17:12 UTC; (mid) 23 Sep 2017 at 18:07 UTC; and (bot) 24 Sep 2017 at 18:17 UTC. P-3 measurement of 10 m referenced wind speed by Stepped Frequency Microwave Radiometer shown in green. CYGNSS 10 m referenced wind speed measurements shown with 1 sec (red dashed) and 4 sec (solid blue) time averaging.*

tracks is several minutes for CYGNSS vs. several tens of minutes for the P-3. For these reasons, an alternative to direct point-by-point comparisons is considered for a quantitative performance assessment.

The top-down performance assessment of CYGNSS retrievals at low to moderate wind speeds made use of the fact that gridded NWP products, reported at regular time intervals, could be interpolated to the time and place of CYGNSS observations. The point-by-point RMS differences between them were used in the top-down assessment reported above. For the comparison between CYGNSS and SFMR winds during hurricane overpasses, such an approach is more problematic for several reasons. The sparse sampling in time and space of SFMR data is less amenable to interpolation and the conditions in and near the storm centers are much more variable over short distances and time differences. For these reasons, rather than using a point-by-point RMS difference,

the expected value of the RMS difference is evaluated statistically by considering the individual histograms of wind speeds measured by the two sensors as proxies for their probability density functions (PDFs).

The RMS difference between CYGNSS and SFMR wind speed measurements in tropical cyclones can be expressed as

$$\varepsilon_{TC} = \left(\int_U (u_{CYG} - u_{SFMR})^2 p(u_{CYG}, u_{SFMR}) du \right)^{0.5} \quad (4)$$

where u_{CYG} and u_{SFMR} are the wind speed measurements made by CYGNSS and SFMR, respectively, $p(u_{CYG}, u_{SFMR})$ is their joint PDF, and the integral is performed over the range of wind speeds, U, for which the RMS difference is evaluated. The squared-difference in eqn. (4) can be expanded and the expected value of its terms evaluated individually, giving

$$\varepsilon_{TC} = (<u_{CYG}^2> - 2 <u_{CYG}><u_{SFMR}> + <u_{SFMR}^2>)^{0.5} \quad (5)$$

where

$$<u_{CYG}> = \int_U u_{CYG} p(u_{CYG}) du \quad (6a)$$

$$<u_{SFMR}> = \int_U u_{SFMR} p(u_{SFMR}) du \quad (6b)$$

$$<u_{CYG}^2> = \int_U u_{CYG}^2 p(u_{CYG}) du \quad (6c)$$

$$<u_{SFMR}^2> = \int_U u_{SFMR}^2 p(u_{SFMR}) du \quad (6d)$$

where $p(u_{CYG})$ and $p(u_{SFMR})$ are the individual PDFs of the two wind speeds. It is assumed that they are independent so their joint PDF is separable. Normalized versions of the histograms of wind speed samples taken by SFMR and CYGNSS during the hurricane overpasses are shown in Fig. 10. They are used as proxies for the PDFs appearing in eqn. (6).

Two versions of the CYGNSS wind speed are considered – one with native 1 sec time averaging and one with an additional 4 sec running average applied in ground processing. Examples of the two versions were shown in Fig. 9 during
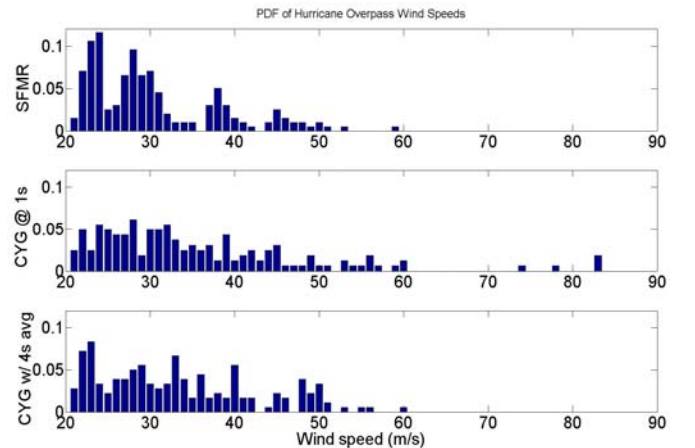

Fig. 10. *Estimates of wind speed probability density function derived from histograms of wind speed sampled by SFMR and CYGNSS during coincident hurricane overpasses. Two versions of the CYGNSS PDF are shown, with native 1 sec time averaging (mid), and with 4 sec time averaging (bot).*

This article has been accepted for inclusion in a future issue of this journal. Content is final as presented, with the exception of pagination.

9

IEEE JOURNAL OF SELECTED TOPICS IN APPLIED EARTH OBSERVATIONS AND REMOTE SENSING

hurricane overpasses. PDFs derived from the wind speed measurements in each case are shown in Fig. 10. Note in Fig. 10 that, with 1 sec averaging, there are some CYGNSS measurements at wind speeds much higher than the maximum SFMR observations, and the distribution of wind speeds sampled is generally more uniformly distributed than that of the SFMR PDF. Both of these characteristics can be attributed to the large additive noise that is present in the measurements with 1 sec time averaging. With 4 sec time averaging, on the other hand, the anomalously high wind speed values have been averaged out and the distribution of measurements at lower wind speed values is generally less uniform and more similar to that of the SFMR distribution.

The RMS difference between SFMR and CYGNSS measurements can be estimated using eqns. (5) and (6) and the PDFs derived from the histograms. The result with 1 sec averaging is 6.75 m/s and with 4 sec averaging is 6.45 m/s. Note that: a) the value of observed RMS difference with 4-s averaging is higher than that predicted by the bottom-up approach; and b) the decrease in observed RMS difference due to averaging is smaller than predicted. Both of these characteristics can be explained by assuming that a significant level of additional intrinsic retrieval error is present, above that assumed in the case of fully developed seas. The additional intrinsic error is likely at least in part a result of the rather ad hoc approach taken by the L2 retrieval algorithm which partitions the sea state into two distinct regimes, fully developed seas and young seas with limited fetch. In reality, fetch length and sea age are continuously varying sea state conditions and the simplifying approach taken by the retrieval algorithm can be expected to introduce additional errors. Generalization of the current algorithm approach to more accurately incorporate variations in sea age and fetch length, in general and near tropical cyclones in particular, is a continuing topic of research by the CYGNSS project team.

C. Rolled up performance assessment

The overall top-down RMS difference between CYGNSS and ECMWF wind speeds, including all coincident matchup samples for which ECMWF winds are less than or equal to 20 m/s, was found to be 1.96 m/s. Note that this value includes components of error due to both CYGNSS and ECMWF uncertainty as well as interpolation errors associated with estimating ECMWF winds at the time and place of the CYGNSS samples. As such, it should be considered an upper bound on the uncertainty in the CYGNSS values. The uncertainty in ECMWF reported wind speeds has been assessed by intercomparisons with a large number of deep water NDBC buoy measurements during 1979-2009 [19]. The RMS error in ECMWF reanalysis winds over the tropics was found to be 1.33 m/s. If this error is removed from the overall 1.96 RMS difference (using root-difference-square subtraction), the remaining uncertainty in the CYGNSS wind speed is 1.44 m/s.

The top-down RMS difference between CYGNSS and SFMR wind speeds, including matchups taken during mutual hurricane overpasses and using samples for which SFMR

winds are greater than or equal to 20 m/s, was found to be 6.45 m/s with 4 sec time averaging of the CYGNSS data. For this sample population, the average SFMR wind speed was 29.35 m/s. As in the lower wind speed case, this value should be considered an upper bound on CYGNSS uncertainty because the RMS difference statistic also includes errors in the SFMR measurement of wind speed and the effects of temporal and spatial decorrelation because the two measurements are not made at exactly the same time and place. The uncertainty in SFMR reported wind speeds up to 70 m/s has been assessed by intercomparisons with 186 coincident dropwindsonde measurements made on 70 hurricane hunter aircraft flights during the 2005 Atlantic hurricane season [18]. The RMS difference between SFMR and dropsindsonde 10 m referenced wind speeds was found to be 4 m/s. If this error is removed from the overall 6.45 RMS difference (using root-difference-square subtraction), the remaining uncertainty in the CYGNSS wind speed is 5.01 m/s. As a fraction of the average SFMR wind speed of 29.35 m/s, the high wind CYGNSS retrieval uncertainty is 17.2%.

IV. DISCUSSION

Bottom-up and top-down approaches to assessing the uncertainty in CYGNSS wind speed measurements show some similarities and some differences, both of which provide some insight into the characterization of performance. At low-to-moderate wind speeds using the retrieval algorithm based on a fully developed seas geophysical model function (GMF), the agreement between bottom-up model predictions and top-down empirical comparisons with "ground truth" winds is generally good, both in terms of the absolute value of the RMS uncertainty and the relative dependence of the uncertainty on wind speed. Below ~15 m/s, the retrieval error grows slowly with wind speed as the sensitivity of the measurements to wind speed (the slope of the GMF) decreases. Above 15 m/s, retrieval error increases more rapidly, both because of a further decrease in sensitivity and an increase in the retrieval bias (the mean difference between retrieved and ground truth wind speeds). A lower sensitivity on the part of the L1 observable to changes in high wind speeds produces larger random errors due to measurement noise as well as larger biases in the retrieved wind speed due to calibration offsets. It is hoped that future refinements in instrument calibration will lower the L1 bias, decrease the resulting L2 wind speed bias, and, ultimately, improve the overall uncertainty.

The GMF used by the CYGNSS wind speed retrieval algorithm is constructed from ECMWF and SFMR u_{10} winds at low and high wind speeds, respectively. Both of these report actual 10 m referenced values, whereas the CYGNSS scattering measurements, which are sensitive to surface roughness forced by wind stress, should be more directly related to the equivalent neutral wind speed [20], [21]. The difference between the actual and equivalent neutral wind speeds is estimated to be 0.2 m/s globally [22], [23], and this difference will contribute to the error in CYGNSS retrievals of

This article has been accepted for inclusion in a future issue of this journal. Content is final as presented, with the exception of pagination.

10

IEEE JOURNAL OF SELECTED TOPICS IN APPLIED EARTH OBSERVATIONS AND REMOTE SENSING

actual wind speed. A possible future refinement for CYGNSS is the retrieval of 10 m equivalent neutral wind speed, similar to the practice in ocean wind scatterometry, to eliminate this source of error.

The discrepancy between bottom-up and top-down performance estimates is larger at high wind speeds using the retrieval algorithm based on the young seas/limited fetch GMF. The bottom-up model predicts that retrieval noise can be significantly reduced by time averaging of the data, and this is borne out by the behavior of the observations. Individual measurements are made with a 1 sec average. Additional time averaging is performed in ground processing, with 3-5 sec of averaging typically used to produce a wind speed product with 25 km spatial resolution. The discrepancy between bottom-up and top-down performance is likely attributable at least in part to the use of a simplified two-regime approach by the wind speed retrieval algorithm to account for variations in sea age and fetch length in and near tropical cyclones. It uses a single limited fetch GMF when near a storm, without regard for the continuously varying transition that actually occurs from a fully developed state far from the storm center. A more proper, physically based, approach should account for this transition zone and should also consider the variability of sea age, fetch length and the resulting long wave swell within the storm, *e.g.* as a function of storm quadrant. This is also an area of active research by the CYGNSS science team, with the expectation that future versions of the L2 wind speed retrieval algorithm will incorporate ancillary information about the sea state, either by adjusting the GMF or the L1 observables appropriately.

The mission level requirements on wind speed measurement uncertainty are +/- 2 m/s at wind speeds below 20 m/s and +/- 10% above 20 m/s. The top-down performance assessment of 1.4 m/s uncertainty at low-to-moderate wind speeds using the FDS GMF demonstrates that the requirement has been met below 20 m/s. At higher wind speeds, the top-down assessment using the YSLF GMF during hurricane overpasses demonstrates a 17% uncertainty and the requirement has not been met. Future improvements to the retrieval algorithm will focus on two primary sources of error. Calibration of the L1 observables can be improved, most notably by lowering the uncertainty in knowledge of the GPS EIRP through better characterization of the transmitter properties of the GPS constellation of satellites [13]. Improved L1 calibration should ameliorate the increase in retrieval uncertainty that occurs at higher wind speeds because the sensitivity of the L1 observables to changes in wind speed is reduced. At high wind speeds in tropical cyclones, the dependence of the L1 observables on long wave swell, in addition to wind driven capillary waves, is another significant source of retrieval error. Future improvements will attempt to incorporate ancillary sea state information to better account for this sensitivity. The improvement to L1 calibration should improve performance and reduce uncertainty at all wind speeds. An improved sea state-dependent retrieval algorithm should further reduce the uncertainty at high wind speeds. Between those two improvements, the high wind measurement uncertainty of 17% should be lowered closer to the original 10% mission requirement.

REFERENCES

[1] Wentz, F.J., "A well-calibrated ocean algorithm for special sensor microwave/imager,' J. Geophys. Res. – Oceans, 102(C4), 8703-8718, DOI: 10.1029/96JC01751, 1997.
[2] Chang, P.S., L. Li,Wilheit, T.T., "Ocean surface wind speed and direction retrievals from the SSM/I," IEEE Trans. Geosci. Remote Sens., 36(6), 1866-1871, DOI: 10.1109/36.729357, 1998.
[3] Chakraborty , A., R. Kumar, A. Stoffelen, "Validation of Ocean Surface Winds from the OCEANSAT-2 Scatterometer Using Triple Collocation," Remote Sensing Ltrs,, 4(1), 84-93, DOI: 10.1080/2150704X.2012.693967, 2013.
[4] Wentz, F.J., L. Ricciardulli, E. Rodriguez, B.W. Stiles, M.A. Bourassa, D.G. Long, R.N. Hoffman, A. Stoffelen, A. Verhoef, L.W. O'Neill, J.T. Farrar, D. Vandemark, A.G. Fore, S.M. Hristova-Veleva, F.J. Turk, R. Gaston, and D. Tyle, "Evaluating and Extending the Ocean Wind Climate Data Record," IEEE J. Sel. Topics Appl. Earth Obs. Remote Sens, 10(5) 2165 – 2185, DOI: 10.1109/JSTARS.2016.2643641, 2017.
[5] Gleason, S., "Space-Based GNSS Scatterometry: Ocean Wind Sensing Using an Empirically Calibrated Model," IEEE Trans. Geosci. Remote Sens., 51(9), doi: 10.1109/TGRS.2012.2230401, 2013.
[6] Foti, G., C. Gommenginger, P. Jales, M. Unwin, A. Shaw, C. Robertson, and J. Roselló, "Spaceborne GNSS Reflectometry for Ocean Winds: First Results from the UK TechDemoSat-1 Mission," Geophys. Res. Lett., 42, 5435–5441, doi:10.1002/2015GL064204, 2015.
[7] Ruf, C. S., R. Atlas, P. S. Chang, M. P. Clarizia, J. L. Garrison, S. Gleason, S. J. Katzberg, Z. Jelenak, J. T. Johnson, S. J. Majumdar, A. O'Brien, D. J. Posselt, A. J. Ridley, R. J. Rose, V. U. Zavorotny," New Ocean Winds Satellite Mission to Probe Hurricanes and Tropical Convection," Bull. Amer. Meteor. Soc., 385-395, March 2016, doi:10.1175/BAMS-D-14-00218.1.
[8] Ruf, C., M. Unwin, J. Dickinson, R. Rose, D. Rose, M. Vincent, A. Lyons, "CYGNSS: Enabling the Future of Hurricane Prediction," IEEE Geosci. Remote Sens. Mag., 1(2), 52-67, doi: 10.1109/MGRS.2013.2260911, 2013.
[9] Gleason, S., C. Ruf, M. P. Clarizia, A. O'Brien, "Calibration and Unwrapping of the Normalized Scattering Cross Section for the Cyclone Global Navigation Satellite System (CYGNSS)," IEEE Trans. Geosci. Remote Sens., 54(5), 2495-2509, doi:10.1109/TGRS.2015.2502245, 2016.
[10] Gleason., S., C. Ruf, A. O'Brien, Darren McKague, "The CYGNSS Level 1 Calibration Algorithm and Error Analysis Based On On-Orbit Measurements" IEEE J. Sel. Topics Appl. Earth Observ. Remote Sens., this issue.
[11] Clarizia, M. P., and C. S. Ruf, "Wind Speed Retrieval Algorithm for the Cyclone Global Navigation Satellite System (CYGNSS) Mission," IEEE Trans Geosci. Remote Sens., 54(8), doi:10.1109/TGRS.2016.2541343, Aug. 2016.
[12] Ruf, C., P. Chang, M.P. Clarizia, S. Gleason, Z. Jelenak, J. Murray, M. Morris, S. Musko, D. Posselt, D. Provost, D. Starkenburg, V. Zavorotny. CYGNSS Handbook, Ann Arbor, MI, Michigan Pub., ISBN 978-1-60785-380-0, 154 pp, 1 Apr 2016.
[13] Wang, T., C.S. Ruf, B. Block, D.S. McKague, S. Gleason, "Design and Performance of a GPS Constellation Power Monitor System for Improved CYGNSS L1B Calibration," IEEE J. Sel. Topics Appl. Earth Observ. Remote Sens., this issue.
[14] Ruf, C., and R. Balasubramaniam, "Development of the CYGNSS Geophysical Model Function for Wind Speed," IEEE J. Sel. Topics Appl. Earth Observ. Remote Sens., this issue.
[15] Clarizia, M. P., Ruf, C., Jales, P. C. Gommenginger, "Spaceborne GNSS-R Minimum Variance Wind Speed Estimator," IEEE Trans Geosci.

This article has been accepted for inclusion in a future issue of this journal. Content is final as presented, with the exception of pagination.

11

IEEE JOURNAL OF SELECTED TOPICS IN APPLIED EARTH OBSERVATIONS AND REMOTE SENSING

Remote Sens., 52(11), 6829-6843, doi:10.1109/TGRS.2014.2303831, Nov. 2014.

[16] Andersson, E., A. Persson, I. Tsonevsky, User Guide to ECMWF Forecast Products, ECMWF, v2.1, 121 pp, 2015.

[17] NOAA, National Centers for Environmental Information, Global Data Assimilation System, https://www.ncdc.noaa.gov/data-access/model-data/model-datasets/global-data-assimilation-system-gdas, 2018

[18] Uhlhorn, E. W., P. G. Black, J. L. Franklin, M. A. Goodberlet, J. R.Carswell, A. S. Goldstein, "Hurricane surface windmeasurements from an operational stepped frequency microwave radiometer," Mon. Wea. Rev., 135, 3070–3085, doi:10.1175/MWR3454.1, 2007.

[19] Stopa, J.E., K.F. Cheung, "Intercomparison of wind and wave data from the ECMWF Reanalysis Interim and the NCEP Climate Forecast System Reanalysis," Ocean Modeling, 75, 65-83, 2014.

[20] Verspeek, J., A. Stoffelen, M. Portabella, H. Bonekamp, C. Anderson, and J. Figa Saldaña, "Validation and calibration of ASCAT using CMOD5.n," IEEE Trans. Geosci. Remote Sens., 48(1), 386-395, 2010.

[21] Ebuchi, N., "Evaluation of marine surface wind speed observed by AMSR2 on GCOM-W," IEEE J. Sel. Topics Appl. Earth Observ. Remote Sens., vol. 10, no. 9, pp. 3955- 3962, doi: 10.1109/JSTARS.2017.2685432, 2017.

[22] Hersbach, H., "CMOD5.N: A C-band geophysical model function for equivalent neutral wind," Technical Memorandum, ECMWF, no. 554, 22 pp., 2008.

[23] Verhoef, A., M. Portabella, A. Stoffelen, and H. Hersbach, "CMOD5.n— The CMOD5 GMF for Neutral Winds," EUMETSAT Tech. Note, SAF/OSI/CDOP/KNMI/TEC/TN/165, 13 pp., 2008.

Christopher S. Ruf (SM'85–M'87–SM'92–F'01) received the B.A. degree in physics from Reed College, Portland, OR ('82), and the Ph.D. degree in electrical and computer engineering from the University of Massachusetts at Amherst ('87). He is currently Professor of atmospheric science and space engineering at the University of Michigan; and Principal Investigator of the NASA Cyclone Global Navigation Satellite System mission. He has worked previously at Intel Corporation, Hughes Space and Communication, the NASA Jet Propulsion Laboratory, and Penn State University. His research interests include GNSS-R remote sensing, microwave radiometry, atmosphere and ocean geophysical retrieval algorithm development, and sensor technology development. Dr. Ruf is a member of the American Geophysical Union (AGU), the American Meteorological Society (AMS), and Commission F of the Union Radio Scientifique Internationale. He is former Editor-in- Chief of the IEEE Transactions on Geoscience and Remote Sensing and has served on the editorial boards of Radio Science and the Journal of Atmospheric and Oceanic Technology. He has been the recipient of four NASA Certificates of Recognition and seven NASA Group Achievement Awards, as well as the 1997 TGRS Best Paper Award, the 1999 IEEE Resnik Technical Field Award, the 2006 IGARSS Best Paper Award, and the 2014 IEEE GRSS Outstanding Service Award.

Scott Gleason (M'10–SM'11) is a Principal Scientist at the University Corporation for Atmospheric Research. He is a Co-Investigator on the science team and Instrument Scientist for the NASA CYGNSS mission. He received his B.S. degree in Electrical and Computer Engineering from the State University of New York at Buffalo ('91), an M.S. in Engineering from Stanford University ('00) and a Ph.D. from the University of Surrey in England ('06). He has worked in the areas of astronautics, remote sensing and Global Navigation Satellite Systems (GNSS) for over 20 years, including at NASA's Goddard Space Flight Center, Stanford's GPS Laboratory, Surrey Satellite Technology Limited, the National Oceanography Centre, Southampton, Concordia University, and the Southwest Research Institute.

Darren S. McKague (M'08) received the Ph.D. degree in astrophysical, planetary, and atmospheric sciences from the University of Colorado, Boulder, CO, USA, in 2001. He was a Systems Engineer at Ball Aerospace, Boulder, CO, USA, and Raytheon, Aurora, CO, USA, and a Research Scientist at Colorado State University, Fort Collins, CO, USA. He was involved in remote sensing with an emphasis on the development of space-borne microwave remote sensing hardware, passive microwave calibration techniques, and on mathematical inversion techniques for geophysical retrievals. He is an Associate Research Scientist with the Department of Climate and Space Sciences and Engineering, University of Michigan, Ann Arbor, MI, USA. His experience with remote sensing hardware includes systems engineering for several advanced passive and active instrument concepts and the design of the calibration subsystem on the Global Precipitation Mission (GPM) Microwave Imager as well as the development of calibration and intercalibration techniques for the GPM constellation. His algorithm experience includes the development of a near-real time algorithm for the joint retrieval of water vapor profiles, temperature profiles, cloud liquid water path, and surface emissivity for the Advanced Microwave Sounding Unit at Colorado State University, and the development of the precipitation rate, precipitation type, sea ice, and sea surface wind direction algorithms for the risk reduction phase of the Conical scanning Microwave Imager/Sounder.